Hindawi
Advances in Civil Engineering
Volume 2023, Article ID 5111719, 14 pages
https://doi.org/10.1155/2023/5111719

Research Article

Time-Dependent Reliability Analysis of RC Bridges Considering Shrinkage, Creep, Resistance Degradation, and Vehicle Load Flows

Xueping Fan,[1,2] **Heng Zhou**,[2] **and Yuefei Liu**[1,2]

[1]*Key Laboratory of Mechanics on Disaster and Environment in Western China, Lanzhou University, The Ministry of Education of China, Lanzhou 730000, China*
[2]*School of Civil Engineering and Mechanics, Lanzhou University, Lanzhou 730000, China*

Correspondence should be addressed to Xueping Fan; fanxp@lzu.edu.cn

Received 20 December 2022; Revised 7 June 2023; Accepted 21 June 2023; Published 8 August 2023

Academic Editor: Claudio Mazzotti

Due to concrete shrinkage, concrete creep, resistance degradation, and vehicle load flows, the long-term performance of reinforced concrete bridges exhibits time-varying characteristics. The vehicle-borne process is a nonstationary random process, which interacts with concrete shrinkage, concrete creep, and resistance degradation to cause constant changes in bridge internal force and deformation, further, bridge dynamic reliability occurs. This study presented a reasonable method for calculating the time-varying reliability of simply supported girder bridges under the effects of traffic loads and shrinkage creep. Stochastic truck-load models were simulated based on site-specific weigh-in-motion measurements, then the internal forces of the bridge were calculated when the mean value of vehicle-mounted effects increases by 1% per year. Considering the resistance degradation and load effect increase, the reliability of the RC bridge in serviceability limit state and capacity-carrying ultimate state were analyzed using first-passage probability method and Monte Carlo method, respectively. The accuracy of the proposed method was verified by comparison. The evaluation results show that the failure probability including shrinkage and creep has increased significantly; creep is affected by the bridge span and the number of main girders, and the reliability assessment results are safer for bridges with smaller spans.

1. Introduction

With the booming transportation market, the current road freight volume has grown significantly. Existing highway bridges are facing a continuous increase in traffic flows and vehicle loads, and the long-term effects will pose a risk to the normal use and safety performance of the bridge. As a result, the service life of bridge will decrease rapidly. To optimize and manage the available budget for repair and maintenance, there is a need for rational decision-making methods and more accurate methods of safety assessment. Reliability or failure probability-based decision-making is a powerful methodology for such optimization. In recent times, probabilistic- and reliability-based approaches have been widely used to quantify bridge safety.

Shrinkage and creep, as the aging behaviors of concrete, will cause additional deformation of RC bridges over time which will cause internal force redistribution and deformation. Further, the unfavorable effects such as the cracking of RC bridge decks and the loss of prestress will be produced which will affect RC bridge durability. Therefore, it is necessary to study the shrinkage and creep effects of RC bridges. In the existing creep analysis [1, 2], the coupling effects of concrete creep, softening, and cracking on deflection evolution and stress redistribution are often ignored. Guo et al. [3] studied the deflection of the prestressed-concrete box girder bridge considering the effects of creep and shrinkage, but in the analysis process, only the creep under the bridge's weight is considered, and the static vehicle load is used to simulate the traffic load. Lu et al. [4] proposed a Gaussian process response surface method based on the dichotomous concept. This method can predict the equivalent stiffness of steel pipe concrete arch ribs under the influence of temperature and shrinkage creep, and obtain the time-varying degradation

law of the mechanical properties of the ribs, which provides a means to analyze the structural performance and time-varying reliability of steel pipe concrete arch bridges under shrinkage creep conditions. To study the reliability analysis of a real-complex structure, the uncertain influence of shrinkage creep is considered, Tonelli et al. [5] based on health monitoring data of a prestressed concrete bridge, performed Bayesian inference using a Markov Chain Monte Carlo (MCMC) method, and the reliability assessment utilizes importance sampling (IS) for computational efficiency.

In the long-term service processes of existing bridges, the structural resistance constantly decaying and the load effect increases gradually with time, so it is more reasonable to use the time-variant reliability as an index to assess and predict structural performance. In the previous studies about structural resistance degradation, the process is usually described in terms of a degradation function [6]. Fan et al. [7] proposed a method based on Bayes theory and resistance degradation model to update bridge resistance. Yuan et al. [8] considered resistance deterioration process, and proposed a time-dependent reliability assessment procedure, the study discussed the nonstationarities of the vehicle-load process, simultaneously.

Vehicle load study is very important for bridge load-carrying capacity calculation, bridge-reliability assessment and life prediction, etc. It is concerned with all phases of bridge design, operation, and maintenance. In the existing studies on the traffic loadings, to simplify the analysis, the traffic loads are usually simplified to a stationary random process [9]. While considering the phase increase of traffic volume, fatigue damage accumulation is a critical factor resulting in the failure of RC bridges. Luo et al. [10] researched the coupled effect of cyclic vehicle loading and environmental corrosion, and the numerical results provide a theoretical basis for fatigue life estimation and maintenance of aging PC bridges. For engineering problems, Kim and Song [11] present a time-varying reliability assessment method for post-tensioned concrete box girder bridges considering traffic-load effects and material deterioration, and applied the method to evaluate the time-varying reliability of the Hwayang–Jobal bridge. Li et al. [12] used ANSYS software to build the finite element method (FEM) simulation model of one main span of the prototype bridge, then the dynamic reliability when the heavy vehicles crossing the prototype bridge corresponding to the middle-span web plate is comprehensively analyzed and discussed. In addition, some progress has been made in recent years on the reliability of bridge structural systems [13–17], and time-varying reliability analysis based on bridge health monitoring data [18–22].

In order to simulate the real-traffic loads and solve the time-variant reliability of RC bridges considering the shrinkage and creep effects of concrete during the service periods, this paper first simulates random traffic flow based on the existing monitored weigh-in-motion (WIM) data, and further combines the FEM to obtain the internal force and deformation of RC bridge. Then time-varying responses of the selected different RC simply supported T-beam bridges are calculated considering the effect of shrinkage and creep. Finally, the reliability analysis method is adopted to predict and assess the safety of the bridge. The flowchart of this study is shown in Figure 1. In the first chapter, based on the probability distribution information of vehicle load, a reasonable random vehicle model is established. On this basis, the second chapter is based on the use of finite element simulation and the use of MATLAB programing, to obtain the internal force response of the bridge. Then the load effect of the bridge is analyzed according to the calculation method of shrinkage and creep in the existing code. Finally, in the third chapter, considering the resistance degradation process, two kinds of time-varying reliability calculation methods are used to analyze the reliability considering the deflection limit and the moment limit, respectively.

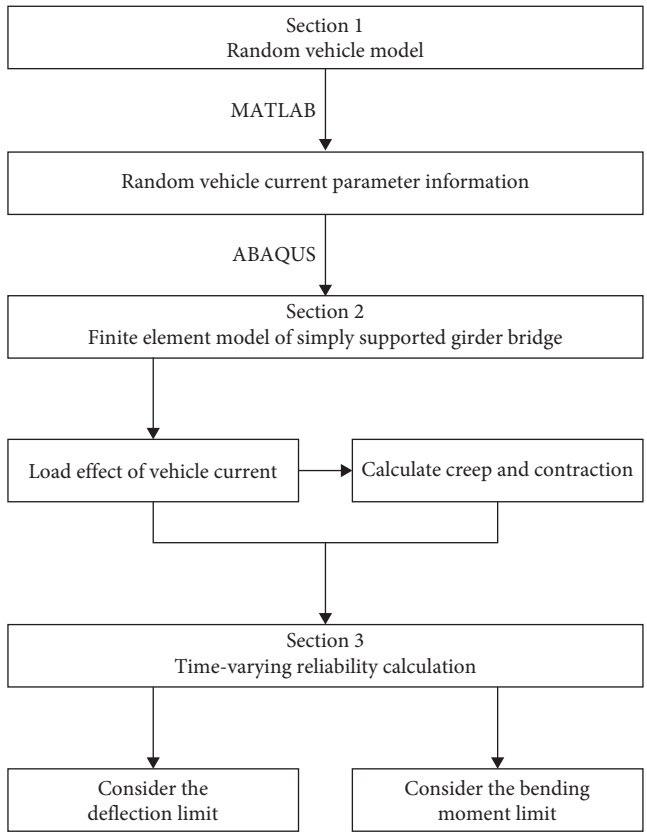

Figure 1: Technical routes of this paper.

2. Random Vehicle Model

In this paper, the random vehicle model considers multiple random parameters including vehicle type, vehicle weight, vehicle distance, and vehicle speed. The random traffic flow is simulated by randomly sampling the vehicle parameter probability model, the research results can provide the foundation for bridge response analysis under the action of the vehicle flows. The analysis flowchart in this section is shown in Figure 2. First, the relevant distribution parameters of each variable are obtained by referring to the existing research data, which can be used to simulate the stochastic traffic flow which is close to the actual traffic load. Then get the sequence of random traffic flow with Monte Carlo method

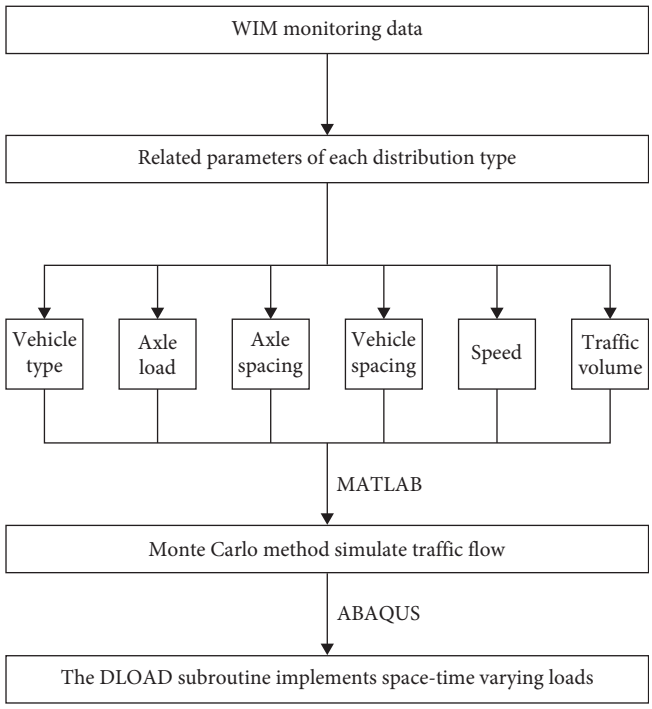

Figure 2: Analysis flowchart of random vehicle model.

by MATLAB. At last, use Fortran language to get the information into the DLOAD subroutine that needs to be executed.

2.1. Statistics-Based Vehicle Probabilistic Model. WIM system is a set of sensor systems installed below the road surface layer to obtain the parameters, such as axle load, vehicle speed, and the passing vehicle types. With the rapid development of sensor technology, the current WIM system has high-control accuracy, and a probabilistic model of the vehicle can be statistically derived from a large amount of statistical data from the WIM system. The daily vehicle number has a certain volatility, and with the increase of service time, the overall trend is increasing.

The statistical research results on the vehicle axle load of highway bridges both show that the highway vehicle loads exhibit multimodal distribution characteristics [23, 24], while the conventional normal distribution and nonnormal distribution only have a single peak. The distribution characteristics cannot accurately fit the total weights and the vehicle axle loads. Therefore, the Gaussian mixture model (GMM) is used to fit the probability distribution of the axle loads [25]. The GMM model is composed of multiple Gaussian functions according to a certain weight. In theory, GMM can fit probability distributions with any shape. The probability density function (PDF) of GMM is:

$$f(x) = \sum_{i=1}^{M} w_i \frac{1}{\sqrt{2\pi}\sigma_i} \exp\left[-\frac{(x-\mu_i)^2}{2\sigma_i^2}\right], \quad (1)$$

where w_i, μ_i, and σ_i are the weight, mean and variance of the ith variable in GMM, respectively. M is the number of Gaussian models.

2.2. Model Parameters. Referring to Lu et al. [26] fitting results of the WIM monitoring data from the NanXi Yangtze River Bridge with four lanes, the passed vehicles are divided into six types (C1–C6) according to the wheel and axle configuration, and the probability characteristic parameters of each vehicle type are statistically obtained and shown in Table 1. The proportion of each vehicle type and the distribution of traffic flow on the four lanes are shown in Figures 3 and 4.

From above statistical parameters, the vehicles crossing the bridge are mainly small passenger cars with two axles, and most of the vehicles are concentrated in the slow lanes on both sides (Lane 1 and Lane 4).

2.3. Distance between Vehicles. The probability distribution of vehicle distance varies greatly with time, and the distribution of vehicle distance has a significant impact on the dynamic response of RC bridges. In the existing study [27], the vehicle operating states are divided into three types according to the distance between vehicles: sparse state, general state, and dense state, but there is no clear boundary division for these three states at present; Zong et al. [28] suggested dividing the dense and sparse states of the vehicle with a time interval of 2 s. Sun and Sun [29] suggested that if the distance between two adjacent vehicles on the same lane is greater than 500 m, then the superposition of load effects can be ignored. Bailey [30] suggested that in general traffic conditions, the intervehicle distance x depends on the total traffic volume V (the number of vehicles per hour), and the probability distribution function can be expressed as follows:

$$f(x) = \frac{V}{3600 \times 22} \exp\left[-\frac{V}{3600 \times 22}(x - 5.5)\right]. \quad (2)$$

Based on the selected bridge span and vehicle speed, the following classification criteria are adopted in this paper: the distance between vehicles in the dense state is less than 40 m, and the distance between vehicles in the general state is 40–500 m. The vehicle distance is generated by Equation (2), and the bridge responses under general traffic conditions can be studied.

2.4. Vehicle Speed and Vehicle Lane. The speed of the vehicle is related to many factors. In the existing research results, Wang et al. [31] used probability and statistical analysis results to show that the vehicle speed generally follows a normal distribution. In this paper, the analysis is simplified, and the consideration of vehicle speed is set as: the speed of the fast lane is 80 km/hr, the speed of the slow lane is 60 km/hr, and the selected bridges are all two-lane traffic.

According to the distribution parameters of each vehicle type, lane, and vehicle spacing obtained by the above statistical analysis, the random traffic flow is generated by the Monte Carlo method. According to the measured lateral and vertical position distribution of the vehicle, MATLAB is used to generate random numbers of a certain sequence and size. Then the DLOAD subroutine is written which can define the variation of the distributed load amplitude with the coordinates, time, unit number, integration point number, etc. It is mainly used

Table 1: Statistical parameters of six typical vehicles.

Vehicle type	Vehicle axle	Axle load (kN)	Axle distance (m)	Lane proportion (%)			
				Lane 1 (slow)	Lane 2 (fast)	Lane 3 (fast)	Lane 4 (slow)
C1	1	44.9	5	42.29	4.48	6.40	46.83
	2	92					
C2	1	76.6	1.9	45.54	0.98	1.65	51.83
	2		5.3				
	3	119.3					
C3	1	84.1	4.8	45.54	0.98	1.65	51.83
	2	113.8	1.4				
	3						
C4	1	75.7	3.8	48.21	1.31	1.59	48.90
	2	83.3	8.6				
	3	151.6	1.3				
	4						
C5	1	82.8	3.6	51.56	1.17	0.97	46.30
	2	140.5	6.8				
	3	97.8	1.3				
	4		1.3				
	5						
C6	1	76.4	1.7	43.47	0.96	0.97	54.60
	2	102.8	2.7				
	3		7.3				
	4		1.3				
	5	113.1	1.3				
	6						

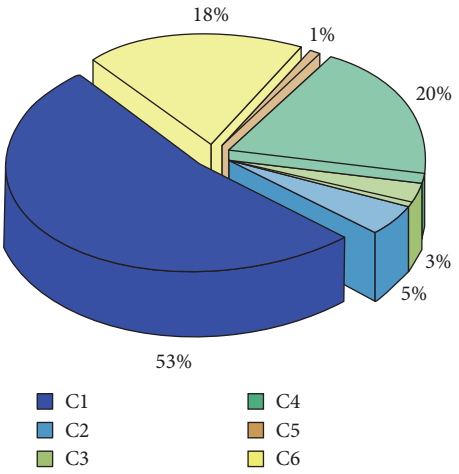

Figure 3: Proportion of six models.

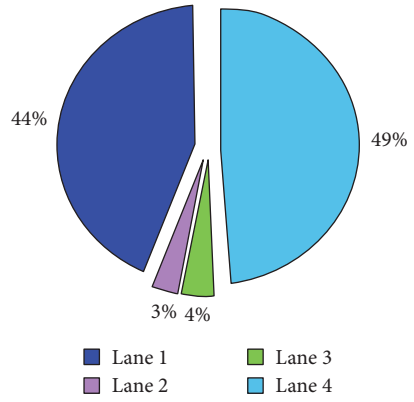

Figure 4: Proportion of vehicle flow in four lanes.

to define complex load conditions. In the subroutine, the random traffic data of the given sequence generated in the previous step is read, so as to realize the time-variant moving random loads on the bridge to simulate the real traffic load flows.

3. Finite Element Model of the Simply Supported Bridge

In order to simulate the above vehicle load effects and calculate the vehicle-axle coupling responses, an example model is established by the finite element software ABAQUS. The concrete is C30, the steel bar is HRB335, and the whole bridge is not equipped with beams; ABAQUS adopts C3D8R element, plastic damage model, and static general analysis step. In order to further explore the influence of shrinkage and creep effects on RC bridges of different bridge types, simply supported T-beam bridges with different span lengths and number of main beams were established. The DLOAD subprogram that had been written was run to calculate the load responses at critical locations of the modeled bridges through ABAQUS software.

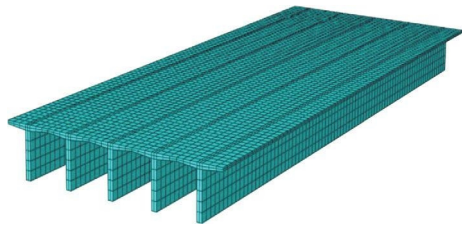

Figure 5: Finite element model of simply supported T-beam bridge.

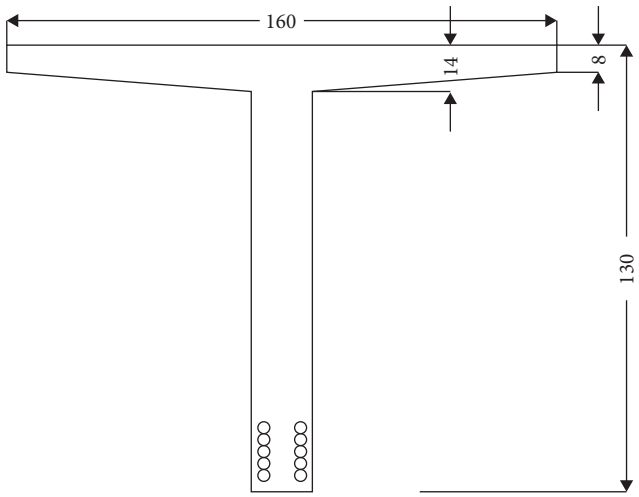

Figure 6: Beam section (unit: cm).

Select four types of spans with spans of 20–50 m and three types with 4–6 main beams to establish a total of 12 bridge types of RC simply supported beam bridge models. The finite element model and the main beam section dimensions are shown in Figures 5 and 6.

In the processes of calculating the bearing capacity, it is necessary to consider the variable load effect, and the dynamic response of the vehicle is usually simplified to the static force by multiplying the corresponding impact coefficient. When calculating the static bending moment (static responses), the load lateral distribution coefficient is introduced. According to the bridge design code in China, the load lateral distribution coefficient is calculated by the orthotropic slab method. Since the actual model of the slab girder bridge is relatively close to be modeled with the orthotropic slab method, the orthotropic slab method is used and has high-calculation accuracy.

The lateral distribution coefficients of midspan loads of bridges with different span lengths and main beam number are calculated. Since the distribution coefficient of the side beams is larger, the most unfavorable case is taken in the calculation. The lateral distribution coefficient of the side beams increases with the increase of the number of main beams, that is, the load borne by the side beams increases. With the increase of the span length, the lateral distribution coefficient gradually decreases which indicates that the lateral distribution of the load is more and more uniform.

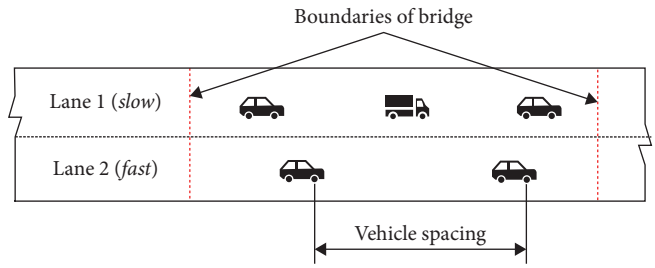

Figure 7: Traffic microsimulation of two lanes of simply supported girder bridges.

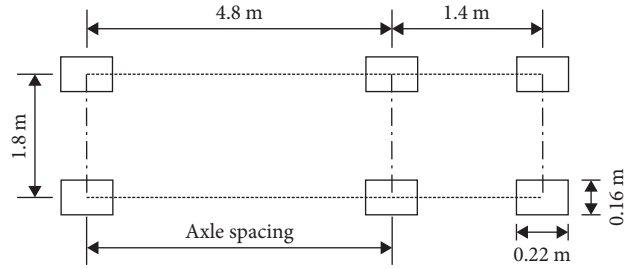

Figure 8: Schematic diagram of typical vehicle load plane.

Figure 7 shows a microscopic simulation of two lanes of traffic on a simple girder bridge after generating a sequence of random traffic flows using Monte Carlo simulation (MCS). In this case, the vehicle speed is set to 80 km/hr in the fast lane (Lane 1) and 60 km/hr in the slow lane (Lane 2). The vehicle spacing is referenced to Equation (2), and judging whether the vehicle is on the bridge by distance and thus applying the load.

Using the C3 model as an example (see Table 1 for axle load, axle spacing, and other information), the plan dimensions of the vehicle load model are shown in Figure 8. This simplification of the wheel-road contact surface to an approximate rectangle is a reference to Liu et al. [32].

4. Time-Variant Reliability Analysis

In structural reliability analysis, the limit states generally include ultimate limit state and serviceability limit state which should be both fully considered. The detailed flowcharts about time-variant reliability for RC bridges are shown in Figure 9.

4.1. Reliability Considering Ultimate Deflection. For the RC bridge, the serviceability limit state usually defines that the dynamic deflection is more than or equal to the maximum allowable deflection. The function G can be expressed as follows:

$$G = y_{\max} - y(t), \tag{3}$$

where $y_{\max}$ is the maximum allowable deflection and $y(t)$ is the time-variant deflection value under variable traffic loads including creep and shrinkage effects.

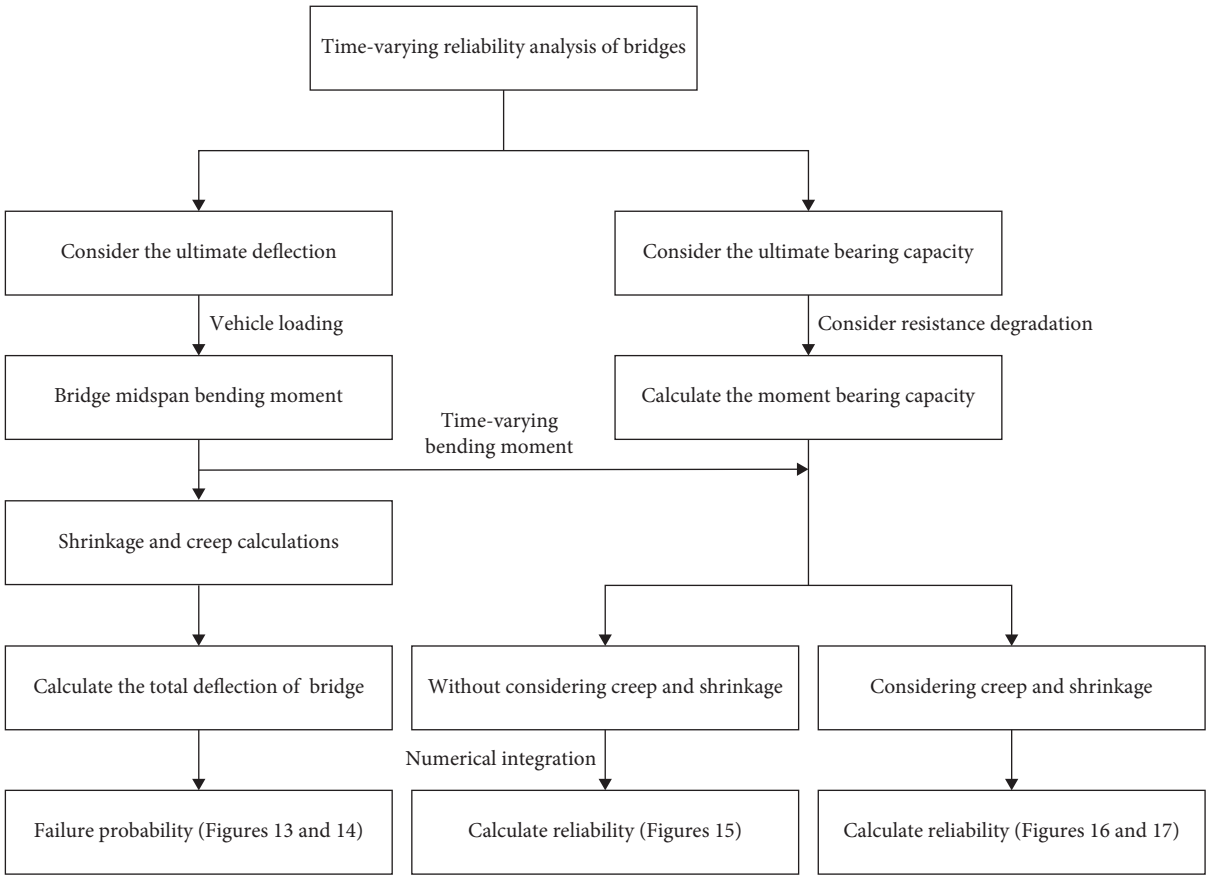

Figure 9: Flowchart of bridge dynamic reliability analysis.

4.1.1. Deflection Calculation. Since the integral calculation about the curvature of each position along the beam is very complicated. For simplifying the calculation, this operation is simplified by assuming parabolic variation between adjacent points. Then, midspan deflection of simply supported beam can be expressed in terms of curvatures at three critical positions: left and right supports and midspan point [33].

$$\Delta_{\text{mid}} \approx \frac{L^2}{96}(k_L + 10k_M + k_R), \tag{4}$$

where L is the span length, k_L, k_M, and k_R are, respectively, the curvatures at the left support, midspan, and right support positions. The total curvature of any section can be obtained from the sum of three components: elastic curvature coefficient $k_{\text{elas}}(t)$, shrinkage curvature coefficient $k_{\text{shrin}}(t, t_s)$, and creep curvature coefficient $k_{\text{cre}}(t, t_0)$ [1]:

$$k(t) = k_{\text{elas}}(t) + k_{\text{cre}}(t, t_0) + k_{\text{shrin}}(t, t_s), \tag{5}$$

where t, t_0, and t_s are, respectively, the calculation time of the curvature coefficient, the age when the concrete starts to creep and the age when the concrete starts to shrinkage. Since the simplified midspan deflection calculation formula is only applicable under the continuous load actions. Further, combining with the FEM, the time-variant deflections of the bridge girder under the random traffic loads are solved.

Assume that there is a continuous average stress or moment for each year, the average is fitted from the applied load effects along the corresponding time period. The long-term load actions are considered as a multi-impulse load process, the time-variant traffic load is decomposed into individual load increments, and then the total curvature is calculated by superimposing the individual responses.

Since the shrinkage coefficient does not change with the load actions. Therefore, at the left and right supports, the curvature coefficient is only caused by the shrinkage coefficient:

$$k_L = k_R = k_{\text{shrin}}(t, t_s). \tag{6}$$

Assume that the elastic part of the deflection $\Delta_{\text{elas(traffic)}}$ is caused by the traffic load at time t, then the calculation formula of the midspan deflection can be expressed as follows:

$$\begin{aligned}\Delta_{\text{mid}} &\approx \frac{L^2}{96}\left\{10\left[k_{\text{elas}}(t) + \sum_i k_{\text{cre}}(t, t_i)\right] + 12k_{\text{shrin}}(t, t_s)\right\} \\ &\approx \Delta_{\text{elas(traffic)}} + \frac{L^2}{96}\left\{10\sum_i k_{\text{cre}}(t, t_i) + 12k_{\text{shrin}}(t, t_s)\right\}.\end{aligned} \tag{7}$$

The FEM is used to impose random traffic loads on the bridge model, and the time-history response of the midspan bending moment is obtained. By fitting the load effects within a certain simulation time, the bending moment value M of the T-beam bridge at the midspan section is obtained and follows extreme value Type I distribution. The elastic deflection can be solved with the following equation:

$$\Delta_{\text{elas(traffic)}} = f = \frac{5}{48} \cdot \frac{ML^2}{B}, \tag{8}$$

where B is the flexural stiffness of the equivalent section of the cracked member [34].

In Equation (7), the calculation formula of the creep curvature coefficient is as follows [35]:

$$k_{\text{cre}} = \frac{k_{\text{elas}}(t_i) \cdot \varphi_{\text{cc}}}{\alpha}, \tag{9}$$

$$k_{\text{elas}}(t_i) = \frac{M(t_i)}{E_c I_{\text{ef}}(t_i)}. \tag{10}$$

In the above formulas, φ_{cc} is the creep coefficient and calculated according to CEB-FIP90 mode, E_c is the concrete young's modulus; the effective moment of inertia I_{ef} is given in term of the ratio of cracked moment M_{cr} to the applied moment $M(t_i)$ [36]:

$$I_{\text{ef}} = \frac{I_{\text{cr}}}{1 - (1 - I_{\text{cr}}/I_{\text{uncr}})(M_{\text{cr}}(t_i)/M(t_i))^2} \le I_{\text{uncr}}, \tag{11}$$

$$\alpha = 0.48\rho^{-0.5}\left(\frac{I_{\text{cr}}}{I_{\text{ef}}}\right)^{0.33}\left[1 + (125\rho + 0.1)\left(\frac{A_{\text{sc}}}{A_{\text{st}}}\right)^{1.2}\right]. \tag{12}$$

In the above formulas, ρ is the reinforcement ratio of the main beam section; A_{sc} and A_{st} are the reinforcement area in the compression zone and the tension zone, respectively.

In Equation (7), the calculation formula of the shrinkage curvature coefficient is

$$k_{\text{shrin}}(t, t_s) = 1.2\left(\frac{I_{\text{cr}}}{I_{\text{ef}}}\right)^{0.67}\left(1 - 0.5\frac{A_{\text{sc}}}{A_{\text{st}}}\right)\left(\frac{\varepsilon_{\text{cs}}(t, t_s)}{h_0}\right), \tag{13}$$

where $\varepsilon_{\text{cs}}(t, t_s)$ is the shrinkage strain given by CEB-FIP90 mode and h_0 is the effective height of the section.

After calculation, the results of the evolution of mean deflection induced by traffic loadings are shown in Figure 10, where the deflection is converted from the annual average bending moment due to traffic loadings.

By substituting the annual average bending moment value $M(t_i)$ following the extreme value Type I distribution and self-weight bending moment into Equations (9)–(13), the deflection caused by shrinkage and creep of the bridge can be obtained as shown in Figures 11 and 12.

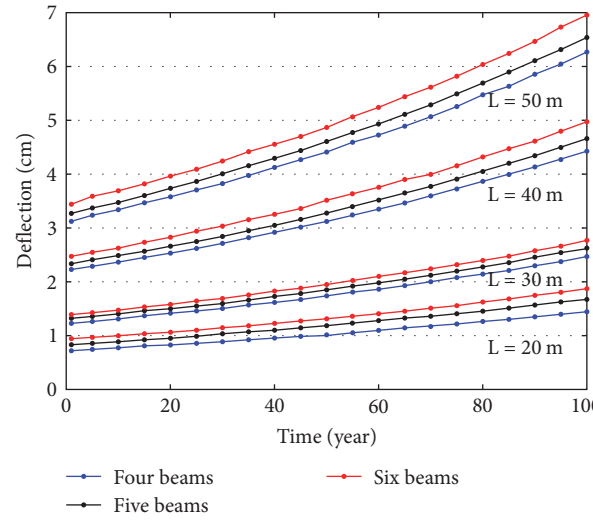

FIGURE 10: Evolution of mean deflection induced by traffic loadings.

Figure 11 shows the time-dependent deflection of a simply supported girder bridge with a span of 20 m caused by shrinkage and creep. The overall value is small, and is like the development trend of shrinkage and creep coefficients: in the early period (the first 10 years) grew rapidly and then gradually slowly. In Figure 12, simply supported girder bridges with different spans with five main girders are selected, and the change trend of creep deflection is also similar. The comparison shows that the deflection value increases with the increase of the number of main beams and the span length.

4.1.2. Monte Carlo Method to Calculate the Failure Probability. With Equations (3) and (7), the performance function about serviceability limit state is expressed as follows:

$$\begin{aligned} G &= y_{\max} - y_{\text{calc}}(t) = \frac{L}{500} - \Delta_{\text{mid}} \\ &= \frac{L}{500} - \Delta_{\text{elas(traffic)}}(t) \\ &\quad - \frac{L^2}{96}\left(10\psi_c \sum_i k_{\text{cre}}(t, t_i) + 12\psi_s k_{\text{shrin}}(t, t_s)\right), \end{aligned} \tag{14}$$

where ψ_c and ψ_s, respectively, represent the modeling errors of the creep coefficient and shrinkage strain. They both follow the normal distribution with the mean 1.0 and the coefficient of variation (0.339 and 0.451, respectively) [15].

Note that the structural performance function value is Z, the random variable X follows the known probability distribution, and the sample value x obtained by sampling is used to calculate the value Z. If $Z<0$, then the structure fails. N simulations are carried out, and there is n_f times appeared for $Z<0$. According to Bernoulli's theorem in probability theory, the frequency of random events $Z<0$ in independent experiments converges to probability p_f, so the estimated value of the structural failure probability p_f is $\widehat{p}_f = n_f/N$. In MATLAB, for each bending moment value M, through

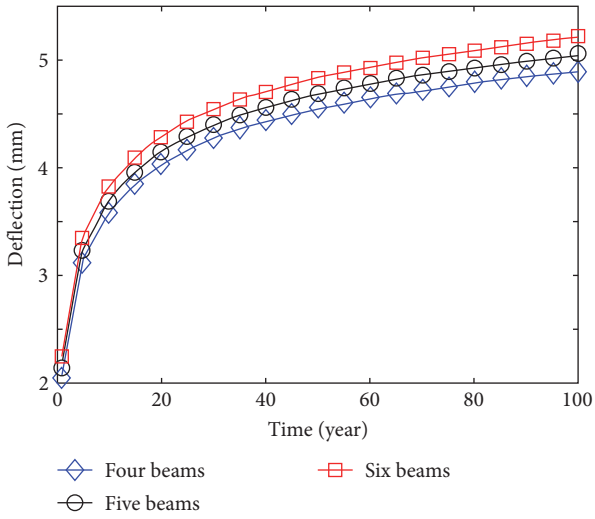

Figure 11: Time-dependent deflection changes of bridges with different numbers of beams due to shrinkage and creep.

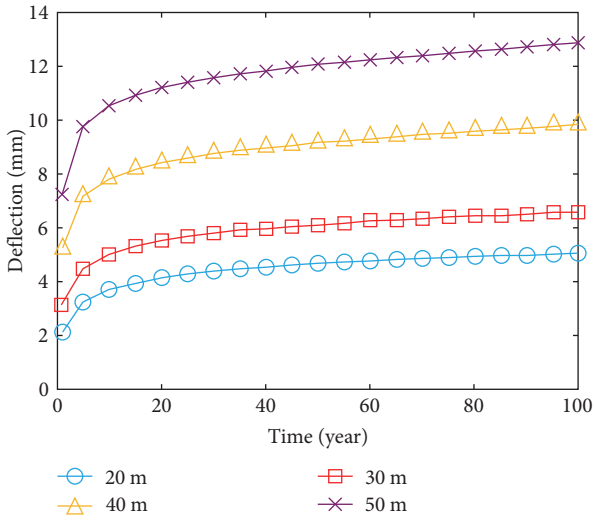

Figure 12: Time-dependent deflection changes of bridges with different beam spans due to shrinkage and creep.

10^6 Monte Carlo numerical simulations, the simulation solutions obtained are shown in Figures 13(a) and 14(a).

Due to the random convergence of MCS, the time-varying reliability is calculated by the first-passage probability method by Andrieu-Renaud et al. [14] to verify the accuracy of the calculation. It is assumed that the structural failure will occur when the dynamic response values (such as the stress, displacement, and acceleration of the control point) exceed the critical value or safety limit for the first time. The more accurate value of time-varying reliability can be obtained by using this method, and the calculated results are shown in Figures 13(b) and 14(b).

It is shown in Figure 14 that the two calculation results are nearly same, which proves the feasibility of this method. Then analyze the trends in the figure. Figure 10 shows the change of failure probability for a 20 m span simply supported beam bridge with allowable deflection as an indicator during the assessment period, it is shown that the failure probability is related to the main girder of the bridge: under the same condition of other parameters, the failure probability of the normal service limit state increases with the increase of the number of the main girder. Figure 11 shows that the failure probability is related to the span of the bridge, and with the increase of the span, the higher the failure probability is, the lower the reliability is. The change trend is like the deflection change caused by the consideration of shrinkage, creep, and vehicle-borne effect, because the increase of the number of main beams and span will cause the increase of the midspan section bending moment value, then the deflection caused by vehicle-borne effect and shrinkage and creep increases. Compared with Figures 8 and 9, the increasing trend of failure probability is steeper during the evaluation period, indicating that the reliability of the bridge in its normal service limit state decreases rapidly with the increasing traffic volume, the potential risk of normal use of existing bridges increases.

4.2. Reliability Considering Ultimate Load-Carrying Capacity. The ultimate load-carrying capacity state means that the structure or component reaches the maximum load-carrying capacity [37]. It is also the frequently considered state in bridge reliability analysis. The flexural load-carrying capacity of the section is regarded as the structural resistance. During the long-term service processes of RC bridges, due to corrosion of steel bars and carbonization of concrete, so the degradation of load-carrying capacity needs to be considered. The degraded time-variant resistance can be expressed as the product of the initial resistance of the member and the resistance degradation function, which is expressed as follows:

$$R(t) = R_0 \cdot g(t), \tag{15}$$

where R_0 is the initial resistance value and calculated according to the relevant bridge design specifications; $g(t)$ is the degradation function of the resistance and described by the piecewise function of the service life T. The resistance degradation function for the medium degradation rate is expressed as follows [6]:

$$g(t) = \begin{cases} 1, & t \leqslant 5 \\ 1 - 0.005(t-5), & t > 5 \end{cases}. \tag{16}$$

For the simply supported girder bridges of medium and short spans, the uncertainty of bridge load effects is mainly originated from the vehicle load which can be described by a discrete random process. According to the measured vehicle data, the vehicle load effects can be simulated and follow the extreme value I type distribution. Further, the cumulative probability function $F(x)$ is obtained. Assume that the vehicle operation is basically stable within 1 year, then the cumulative probability function $F_M(x)$ of the maximum load effects in the design basis period ($T = 100$ years) is expressed as follows:

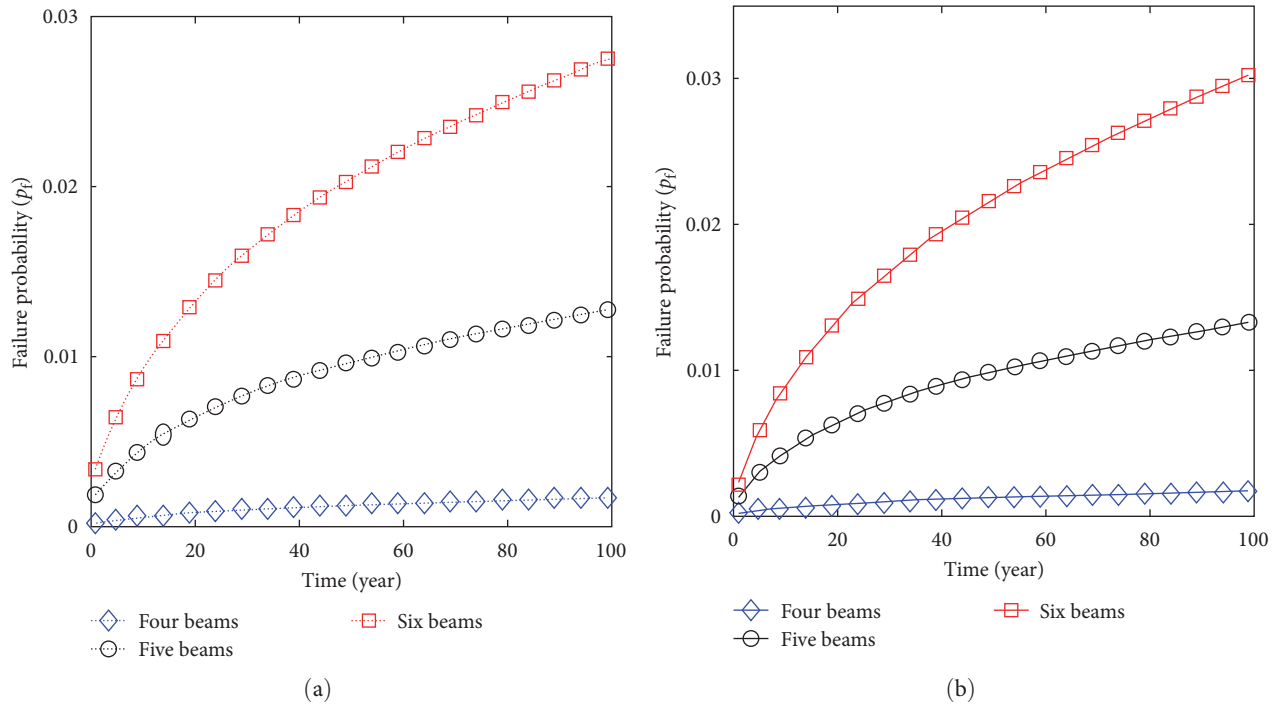

Figure 13: Failure probability of simply supported beam bridges with different number of main beams. (a) Failure probability calculated by MCS. (b) Failure probability calculated by first-passage probability method.

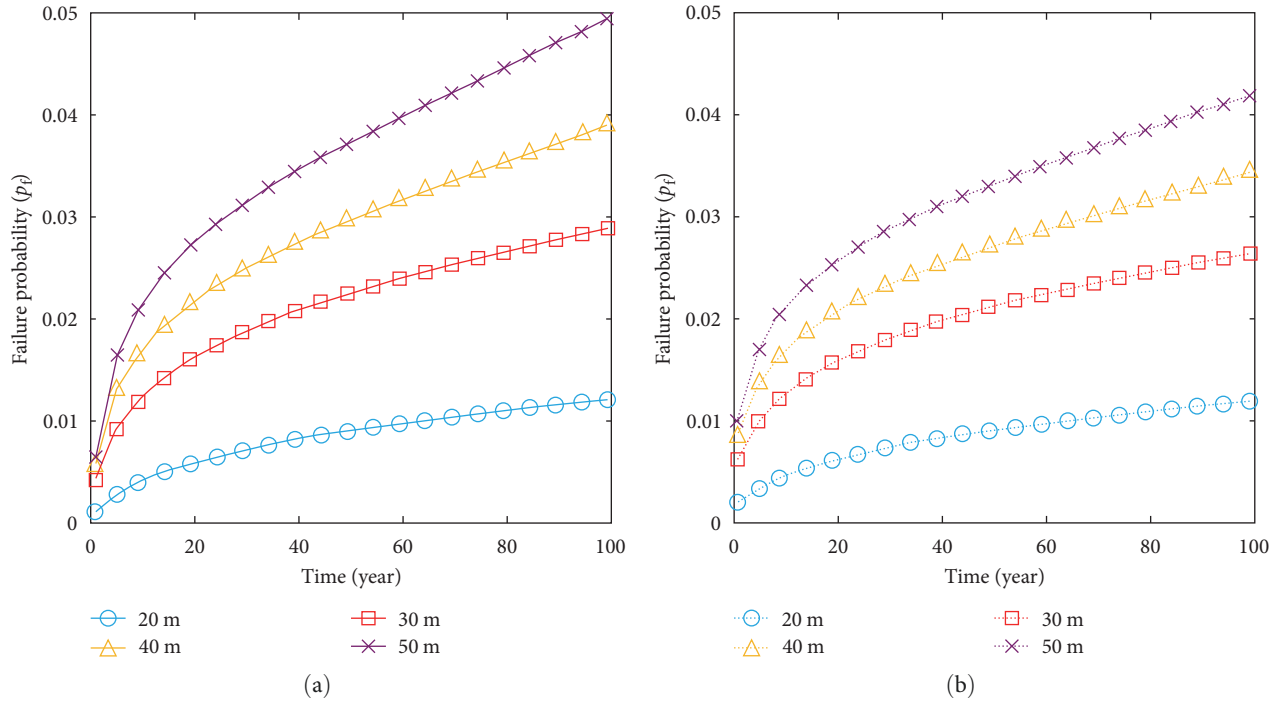

Figure 14: Failure probability of simply supported beam bridges with different spans. (a) Failure probability calculated by MCS. (b) Failure probability calculated by first-passage probability method.

$$F_M(x) = [F(x)]^T = [F(x)]^{100}. \quad (17)$$

4.2.1. Only Consider the Reliability Calculation of the Vehicle. The occurrence process of the vehicle can be regarded as a Poisson process, and the Poisson strength is recorded as λ (the probability that a vehicle occurs once per unit time). If the service time T is divided into n intervals to form a time interval sequence $\{X_n, n = 1, 2,\ldots,\}$, then for the ith $(i = 1, 2,\ldots n)$ time interval X_i, the occurred probability of a vehicle

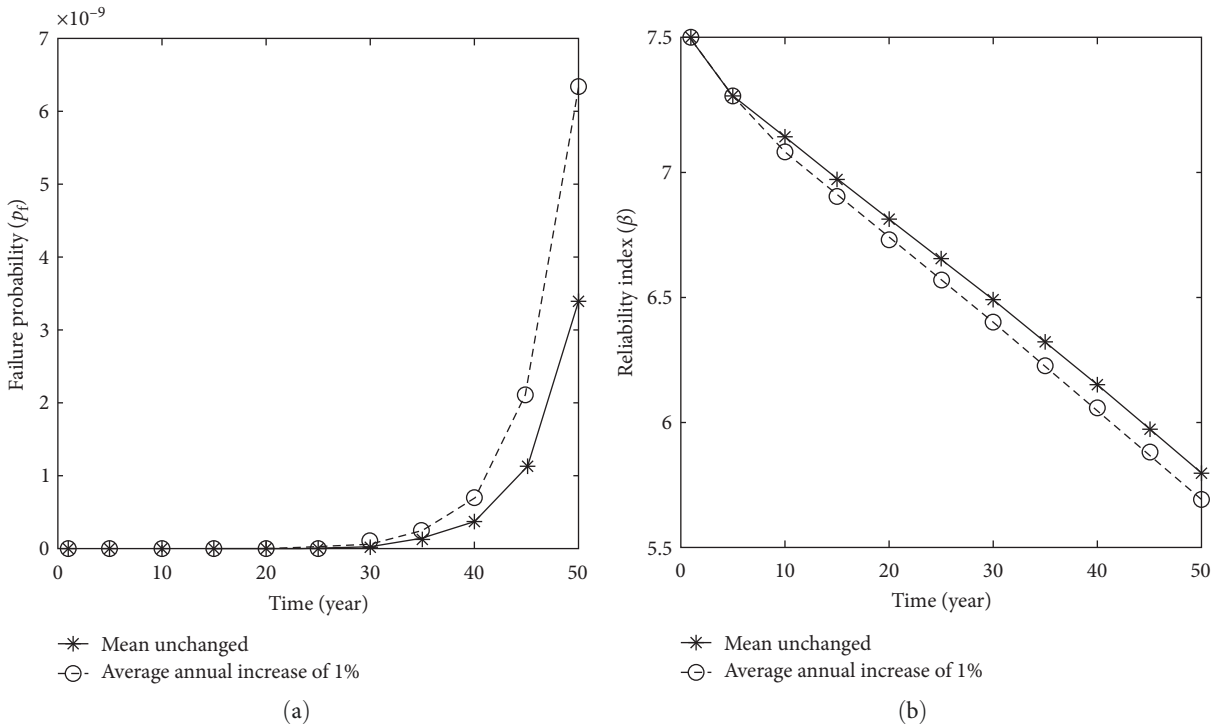

FIGURE 15: Failure probability and reliability indices without considering creep and shrinkage. (a) The failure probability without considering creep and shrinkage. (b) The reliability indices without considering creep and shrinkage.

load is $p = \lambda T/n$. As is considered that the load changes with time, it is assumed that the cumulative density function of the load effect is $F_S(t, s)$. When T/n is sufficiently small, it is assumed that the cumulative density function of the load effect S within X_i remains constant, and is denoted as $F_S(iT/n, s), i = 1, 2\ldots n$. At the same time, considering the randomness of the initial resistance value R_0 and the PDF of which is $f_R(r)$, then the time-varying reliability probability $p_r(T)$ of the structure within $(0, T]$ is defined as follows [38]:

$$\begin{aligned} p_r(T) &= Pr\{R(t) > S(t), t \in (0, T\,]\} \\ &= \int_0^{\infty} \exp\left\{\lambda \int_0^T F_S[t, R_0 \cdot g(t)]dt - \lambda T\right\} \cdot f_R(r)dr, \end{aligned} \tag{18}$$

where $R(t)$ and $S(t)$ represent the structural resistance and load effect at the t moment, respectively. It is usually used as the reliability index β, and its relationship with the reliability probability is $p_r(T) = \Phi(\beta)$.

Statistical analysis on the load-carrying capacity of RC beams shows that the load-carrying capacity follows a log-normal distribution with a coefficient of variation (0.15).

A bridge with a span of 20 m and a number of five main beams is taken as an example, the mean and standard deviation about the maximum bending moment of the midspan section caused by the vehicle loads once-in-a-year ($\lambda = 1$) are 379.067 and 41.187 kN·m, respectively. According to the relevant specifications, excluding the self-weight of the main beam, the midspan flexural load-carrying capacity of the bridge considering the long-term load effects is 1,041.97 kN·m. The load effect S and the load-carrying capacity R, respectively, follow the extreme value type I distribution and log-normal distribution. The PDF of the load-carrying capacity and the cumulative distribution function of the load effect are

$$f_{R_0}(r) = \frac{1}{0.149\sqrt{2\pi}r} \exp\left[-\frac{1}{2}\left(\frac{\ln r - 6.938}{0.149}\right)\right], \tag{19}$$

$$F_S(s) = \exp\left(-\exp\left(-\frac{s - 360.531}{32.113}\right)\right). \tag{20}$$

Assume that the vehicle load effect average value increases with a fixed value every year, and the increment is 1% of the mean value at the initial time. That is, the annual increase of vehicle-load bending moment is 3.79 kN·m, so the function F_S updated with time is

$$F_S(s, t) = \exp\left(-\exp\left(-\frac{s + 3.79t - 360.531}{32.113}\right)\right), \tag{21}$$

where s represents the vehicle load effect and t represents the service time. Substitute Equations (19) and (21) into Equation (18), the failure probability can be calculated and shown in Figure 15.

The results in Figure 15 show that the reliability indices in the first 10 years are basically the same, and the gap gradually increases, but still maintains a small difference in 50 years. The probability is basically the same in the first 25 years, but the overall value has significantly increased after the 40th year. It shows that the evaluation results of the

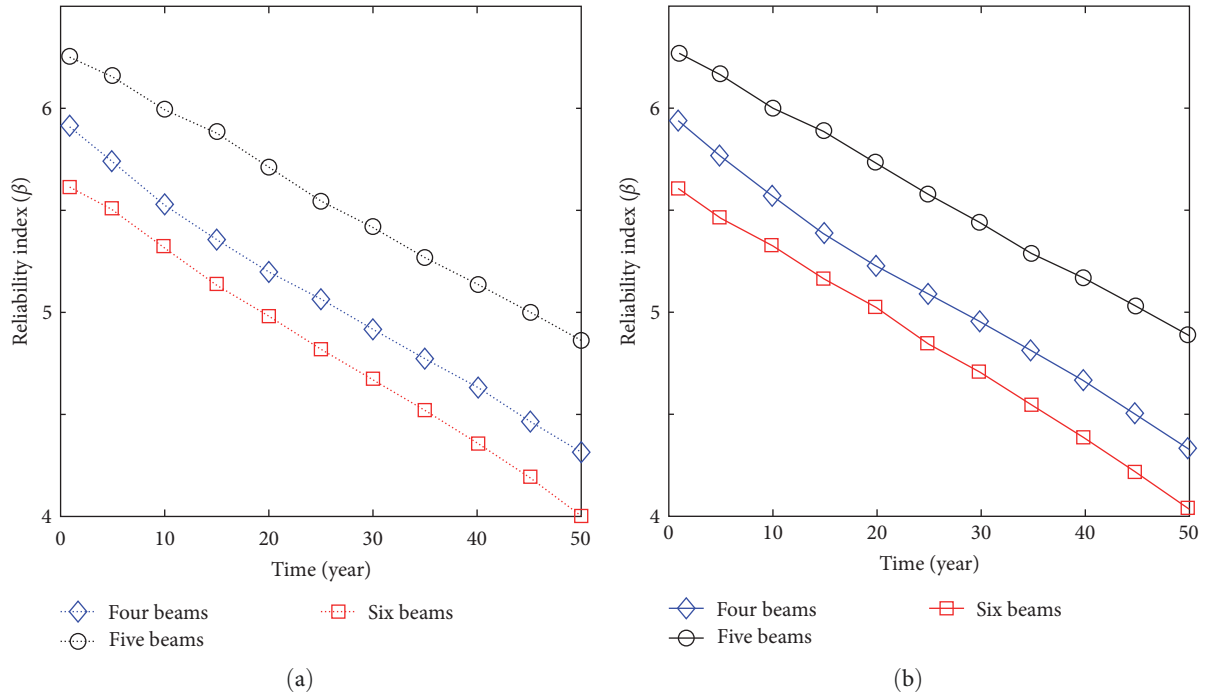

FIGURE 16: Time-varying reliability indices of simply supported beam bridges with different number of main beams. (a) The reliability indices calculated by Monte Carlo method. (b) The reliability indices calculated by first-passage probability method.

simulated bridge with aging and increasing load effect are unsafe and the potential risk is increased.

4.2.2. Reliability Calculation Considering Shrinkage and Creep. In order to compare the time-variant reliability results, the Monte Carlo numerical simulation method was adopted, and the influence of shrinkage and creep was considered, and the time-variant reliability of the structure with the average annual increase of the vehicle (1% of the average value at the initial time) was solved. The detailed steps are described as follow:

Step 1: according to the log-normal distribution of the load-carrying capacity of different bridge types, the value r_0 of the initial load-carrying capacity is randomly generated;

Step 2: Generate 100 time series uniformly distributed over $(0, T]: t_1 < t_2 \ldots < t_{100}$;

Step 3: corresponding to each time interval, the corresponding bending moment value s_i $(i = 1, 2, \ldots, 100)$ is generated according to the updated cumulative distribution function of the vehicle load effect such as Equation (21);

Step 4: according to Equation (8) and using the previously calculated creep deflection, the bending moment values generated by the shrinkage and creep effects can be inversely calculated, each time is corresponding to a creep bending moment $M_{\text{cre}}(i)$;

Step 5: for all $i = 1, 2, \ldots, 100$, if all satisfy $r_0 \cdot g(t_i) \geq s_i + M_{\text{cre}}(i)$, the structure is safe, otherwise it is recorded as the structural failure;

Step 6: repeat the above steps one to five for N times, in which the number of failures is n_f, and the number of simulations is also taken as 10^6, then the failure probability p_f can be estimated from n_f/N.

The accuracy of the calculation is still verified by the first-passage probability method. The results of the simulation method are shown in Figures 13(a) and 14(a), and the result of first-passage probability method are shown in Figures 16(a) and 16(b).

Figures 16 and 17 show the time-dependent reliability of different bridge types, with the bending moment bearing capacity as an indicator. The comparison in Figure 17 shows that the larger the span of simply supported beam bridge is, the lower the reliability index value considering the ultimate bearing capacity is, and the shorter the span is, the safer the bridge is. However, the influence of the number of main beams on the reliability index is not monotonous. With the increase of the number of main beams, the reliability index decreases, however, the calculated value of the flexural capacity is not consistent with the increase of the moment, which results in the highest reliability index of the bridge with five main girders in Figure 16.

Figure 14 also shows that the influence of span length on the reliability index is significant, and the difference of the reliability index between the spans of adjacent bridges becomes larger and larger, which further indicates that the effect of shrinkage and creep is especially sensitive to the change of span length. In addition, compared with the time-dependent reliability in Figure 15(b), which does not include the load effect of shrinkage and creep, the reliability considering the effect of shrinkage and creep is significantly

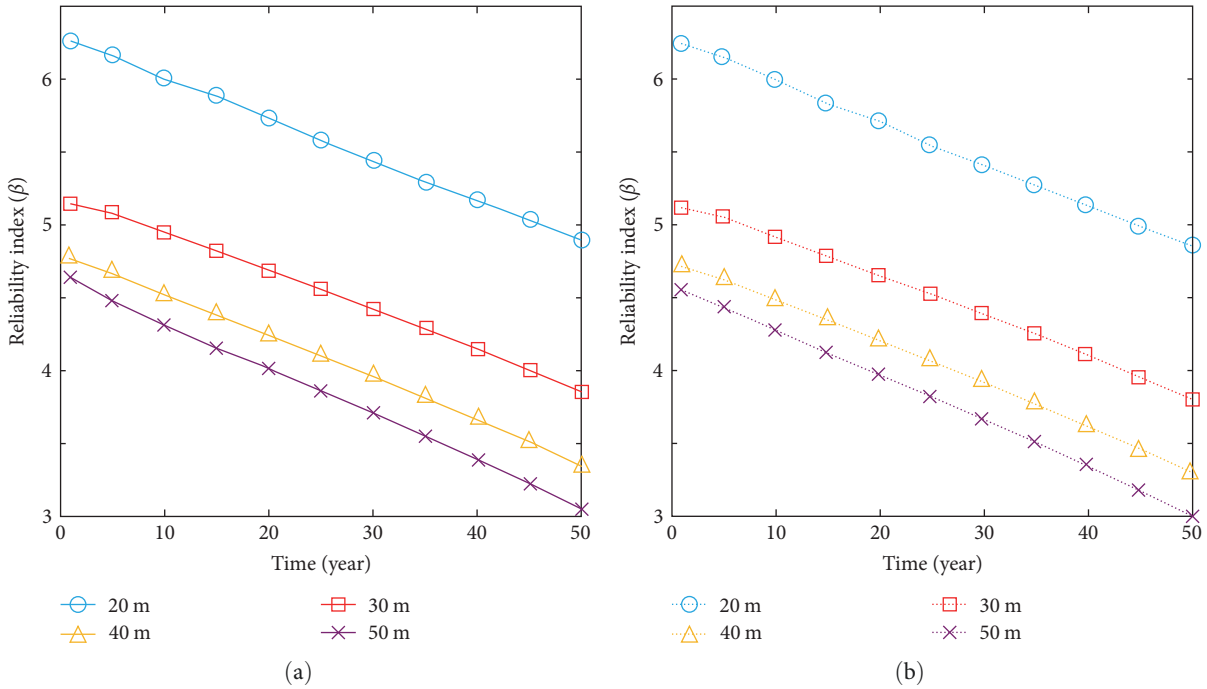

FIGURE 17: Failure probability of simply supported beam bridges with different spans. (a) The reliability indices calculated by Monte Carlo method. (b) The reliability indices calculated by first-passage probability method.

reduced (the initial value is reduced from 7.5 to 6.26), it shows that the creep effect should be fully considered in the reliability analysis of existing concrete bridges. During the evaluation period, the selected examples are safe, but with the increase of service life, the reliability index decreases rapidly, and facing the increasing traffic volume, the long-term load effect of the bridge increases, and the shrinkage and creep effect intensifies, it will bring more risk to the safety of bridge structure.

5. Conclusions

In this study, a simple implementation of a stochastic traffic load model is proposed, which is prepared in Fortran language to read the random traffic flow data generated by MATLAB, and then the numerical simulation results of the internal force response of a simply supported girder bridge are obtained by the FEM. The time-varying reliability analysis was carried out considering the effects of shrinkage, creep, and vehicle loading of the bridge under two limit states. The main conclusions were obtained as follows.

(1) In-service RC bridge condition assessment should fully consider the effects of shrinkage, creep, and structural deterioration. In the numerical example of this paper, the initial value of the reliability index of the bridge after considering shrinkage and creep is reduced from 7.5 to 6.26.

(2) Comparing different bridge types (variables are number of main girders and span diameter), it is shown that shrinkage and creep are significantly affected by the span diameter of the bridge, and the reliability assessment results are safer for the smaller span diameter of the bridge. The number of main girders increases, and the deformation from shrinkage and creep increases, but the reliability of the load-carrying capacity limit state is not monotonically changed.

(3) Compared with the disadvantage of the time-consuming Monte Carlo method, the first-passage probability method can perform time-varying reliability analysis of the structure of complex functional functions with high-computational efficiency and accurate results.

(4) The stochastic vehicle-carrying model proposed in this paper can be adjusted according to the vehicle-carrying probability information of different traffic states, to reasonably analyze and predict the load effect of vehicle flow.

Symbols

B: Flexural stiffness of equivalent sections of cracked members
E_c: Concrete young's modulus at the age of 28 days
G: The performance or limit state function
K_L, K_M, K_R: The curvatures at left support, midspan and right support, respectively
L: The span length
M: Bending moment at the span section of the bridge
R: Resistance of bridge
S: Load effect of bridge.

Notations

A_{sc}: The steel area in compression zone
A_{st}: The area of tensile reinforcement
$g(t)$: Resistance degradation function
h_0: Effective height of cross-section
I_{ef}: The effective moment of inertia
I_{cr}: The cracked moment of inertia
k_{cre}: The curvatures induced by creep
k_{shrin}: The curvatures induced by shrinkage
k_{elas}: The curvatures induced by elastic
M_{cr}: Cracked moment
M_{cre}: Conversion of deformation caused by creep into bending moment
p_f: The failure probability
t_0: The age of concrete at the beginning of creep
t_s: The age at the initiation of shrinkage
y_{max}: The maximum acceptable deflection of bridge
α: Empirical coefficient related to the amount of cracking and reinforcement quantity
β: Reliability index
ε_{cs}: The shrinkage strain
$\Delta_{elas(traffic)}$: The elastic part of the deflection
ρ: The ratio of reinforcement in the web
φ_{cc}: The creep coefficient
ψ_c, ψ_s: The modeling error for the creep coefficient and shrinkage strain, respectively.

Data Availability

Some or all data, models, or code generated or used during the study are available from the corresponding author upon request (list items).

Conflicts of Interest

The authors declare that they have no conflicts of interest.

Acknowledgments

This work was supported by Fundamental Research Funds for the Central Universities (grant no. lzujbky-2022-43) and National Natural Science Foundation of China (grant no. 51608243).

References

[1] E. H. Khor, D. V. Rosowsky, and M. G. Stewart, "Probabilistic analysis of time-dependent deflections of RC flexural members," *Computers & Structures*, vol. 79, no. 16, pp. 1461–1472, 2001.

[2] T. Tong, Z. Liu, J. Zhang, and Q. Yu, "Long-term performance of prestressed concrete bridges under the intertwined effects of concrete damage, static creep and traffic-induced cyclic creep," *Engineering Structures*, vol. 127, pp. 510–524, 2016.

[3] T. Guo, R. Sause, D. M. Frangopol, and A. Li, "Time-dependent reliability of PSC box-girder bridge considering creep, shrinkage, and corrosion," *Journal of Bridge Engineering*, vol. 16, no. 1, pp. 29–43, 2011.

[4] P. Lu, D. Li, T. Hong, Y. Chen, and Q. Shi, "Concrete performance time-varying effect of CFST arch bridges," *Mechanics of Time-Dependent Materials*, vol. 26, no. 2, pp. 377–395, 2022.

[5] D. Tonelli, A. Beltempo, C. Cappello, O. S. Bursi, and D. Zonta, "Reliability analysis of complex structures based on Bayesian inference," *Structural Health Monitoring*, Article ID 147592172311527, 2023.

[6] M. P. Enright and D. M. Frangopol, "Condition prediction of deteriorating concrete bridges using Bayesian updating," *Journal of Structural Engineering*, vol. 125, no. 10, pp. 1118–1125, 1999.

[7] X. P. Fan, S. Wang, and Y. F. Liu, "Bridge resistance updating based on the general particle simulation algorithms of complex Bayesian formulas," *Advanced Engineering Forum*, vol. 43, pp. 111–122, 2021.

[8] Y. Yuan, W. Han, G. Li, Q. Xie, and Q. Guo, "Time-dependent reliability assessment of existing concrete bridges including non-stationary vehicle load and resistance processes," *Engineering Structures*, vol. 197, Article ID 109426, 2019.

[9] H. Xie, Y. Wang, and R. Zou, "Reliability analysis of RC T-beam highway bridges in China based on a virtual bridge dataset," *Engineering Structures*, vol. 104, pp. 133–140, 2015.

[10] Y. Luo, H. Zheng, H. Zhang, and Y. Liu, "Fatigue reliability evaluation of aging prestressed concrete bridge accounting for stochastic traffic loading and resistance degradation," *Advances in Structural Engineering*, vol. 24, no. 13, pp. 3021–3029, 2021.

[11] J. Kim and J. Song, "Time-dependent reliability assessment and updating of post-tensioned concrete box girder bridges considering traffic environment and corrosion," *ASCE-ASME Journal of Risk and Uncertainty in Engineering Systems, Part A: Civil Engineering*, vol. 7, no. 4, Article ID 04021062, 2021.

[12] Y. Li, J. He, X. Zeng, and Y. Tang, "Dynamic reliability assessment of heavy vehicle crossing a prototype bridge deck by using simulation technology and health monitoring data," *Journal of Architectural Environment & Structural Engineering Research*, vol. 5, no. 4, pp. 10–17, 2022.

[13] T. Sun and J. Chen, "Physically driven exact dimension reduction of a class of nonlinear multidimensional systems subjected to additive white noise," *ASCE-ASME Journal of Risk and Uncertainty in Engineering Systems, Part A: Civil Engineering*, vol. 8, no. 2, Article ID 04022012, 2022.

[14] C. Andrieu-Renaud, B. Sudret, and M. Lemaire, "The PHI2 method: a way to compute time-variant reliability," *Reliability Engineering & System Safety*, vol. 84, no. 1, pp. 75–86, 2004.

[15] B. Tu, Z. Fang, Y. Dong, and D. M. Frangopol, "Time-variant reliability analysis of widened deteriorating prestressed concrete bridges considering shrinkage and creep," *Engineering Structures*, vol. 153, pp. 1–16, 2017.

[16] J. Cheng, "Serviceability reliability analysis of prestressed concrete bridges," *KSCE Journal of Civil Engineering*, vol. 17, no. 2, pp. 415–425, 2013.

[17] L. Saad, A. Aissani, A. Chateauneuf, and W. Raphael, "Reliability-based optimization of direct and indirect LCC of RC bridge elements under coupled fatigue-corrosion deterioration processes," *Engineering Failure Analysis*, vol. 59, pp. 570–587, 2016.

[18] P.-P. Li, Z.-H. Lu, and Y.-G. Zhao, "Bayesian updating of time-dependent structural reliability using the method of moment," *ASCE-ASME Journal of Risk and Uncertainty in Engineering Systems, Part A: Civil Engineering*, vol. 7, no. 4, Article ID 04021066, 2021.

[19] Y. Q. Ni and R. Chen, "Strain monitoring based bridge reliability assessment using parametric Bayesian mixture model," *Engineering Structures*, vol. 226, Article ID 111406, 2021.

[20] Q. K. Xiao, Y. P. Liu, L. C. Zhou, Z. J. Liu, Z. Y. Jiang, and L. Q. Tang, "Reliability analysis of bridge girders based on regular vine Gaussian copula model and monitored data," *Structures*, vol. 39, pp. 1063–1073, 2022.

[21] Y. Liu, J. Zhou, J. Su, and J. Zhang, "Residual capacity assessment of in-service concrete box-girder bridges considering traffic growth and structural deterioration," *Structural Engineering and Mechanics*, vol. 85, no. 4, pp. 531–543, 2023.

[22] X. P. Fan and Y. F. Liu, "New dynamic prediction approach for the reliability indexes of bridge members based on SHM data," *Journal of Bridge Engineering*, vol. 23, no. 12, Article ID 06018004, 2018.

[23] T. Guo, A. Q. Li, and D. L. Zhao, "Probabilistic model of vehicle load multimodal distribution for reliability assessment of highway bridges," *Journal of Southeast University: Natural Science Edition*, vol. 38, no. 5, pp. 763–766, 2008.

[24] L. Lu, B. Ji, L. Ma, M. Wang, and G. Shi, "Study on the vibration response of long span suspension bridge based on measured traffic flow," *Chinese Journal of Civil Engineering*, no. S1, pp. 102–108, 2011.

[25] N. Shental, A. Bar-Hillel, T. Hertz, and D. Weinshall, "Computing Gaussian mixture models with EM using equivalence constraints," *Advances in Neural Information Processing Systems*, vol. 2003, pp. 465–472, 2003.

[26] N.-W. Lu, Y. Liu, and X.-H. Xiao, "Extrapolation method of extreme value of load effect of long-span bridge under measured traffic flow," *Chinese Journal of Transportation Engineering*, vol. 18, no. 5, pp. 47–55, 2018.

[27] N. W. Lu and Y. Liu, *Bridge Reliability Analysis Method and Application*, Southeast University Press, Nanjing, 2017.

[28] Z. H. Zong, F. F. Li, Y. F. Xia, and W. W. Yuan, "Research on vehicle load model of Xinyi River Bridge based on WIM," *Bridge Construction*, vol. 43, no. 5, pp. 29–36, 2013.

[29] S. W. Sun and L. M. Sun, "Statistical model of vehicle load on highway bridges based on actual measurement," *Journal of Tongji University: Natural Science Edition*, vol. 40, no. 2, pp. 198–204, 2012.

[30] S. F. Bailey, *Basic Principles and Load Models for the Structural Safety Evaluation of Existing Road Bridges*, EPFL, 1996.

[31] D. Wang, Y. Liu, W. S. Han, and P. M. Huang, "Simulation of random traffic flow on highway bridges," *Journal of China & Foreign Highway*, vol. 29, no. 6, pp. 157–160, 2009.

[32] M. H. Liu, X. M. Huang, and X. H. Tao, "Finite element method analysis of dynamic response of pavement structure near abutment under moving load," *Journal of Highway and Transportation Science and Technology*, vol. 23, no. 5, pp. 1–6, 2006.

[33] F. E. H. Chehade, R. Younes, H. Mroueh, and F. H. Chehade, "Time-dependent reliability analysis for a set of RC T-beam bridges under realistic traffic considering creep and shrinkage," *European Journal of Environmental and Civil Engineering*, pp. 1–25, 2021.

[34] JTG 3362, *Design Code for Highway Reinforced Concrete and Prestressed Concrete Bridges and Culverts*, China Communications Press, Beijing, 2018.

[35] R. I. Gilbert and G. Ranzi, *Time-Dependent Behaviour of Concrete Structures*, CRC Press, 2010.

[36] P. H. Bischoff, "Deflection calculation of FRP reinforced concrete beams based on modifications to the existing Branson equation," *Journal of Composites for Construction*, vol. 11, no. 1, pp. 4–14, 2007.

[37] S. Jamali, T. H. T. Chan, A. Nguyen, and D. P. Thambiratnam, "Reliability-based load-carrying capacity assessment of bridges using structural health monitoring and nonlinear analysis," *Structural Health Monitoring*, vol. 18, no. 1, pp. 20–34, 2019.

[38] C. Wang and Q. W. Li, "Time-varying reliability analysis of in-service bridges considering non-stationary on-board process," *Engineering Mechanics*, vol. 33, no. 3, pp. 18–23, 2016.